The Journal of Chemical Physics

RESEARCH ARTICLE | APRIL 10 2024

Predissociation dynamics of the hydroxyl radical (OH) based on a five-state spectroscopic model

Georgi B. Mitev ; Jonathan Tennyson ; Sergei N. Yurchenko

J. Chem. Phys. 160, 144110 (2024)
https://doi.org/10.1063/5.0198241

AIP Publishing

The Journal of Chemical Physics ARTICLE pubs.aip.org/aip/jcp

Predissociation dynamics of the hydroxyl radical (OH) based on a five-state spectroscopic model

Cite as: J. Chem. Phys. 160, 144110 (2024); doi: 10.1063/5.0198241
Submitted: 17 January 2024 • Accepted: 21 March 2024 •
Published Online: 10 April 2024

Georgi B. Mitev,[a] Jonathan Tennyson,[b] and Sergei N. Yurchenko

AFFILIATIONS

Department of Physics and Astronomy, University College London, Gower St., London WC1E 6BT, United Kingdom

[a]Electronic mail: georgi.mitev.16@ucl.ac.uk
[b]Author to whom correspondence should be addressed: j.tennyson@ucl.ac.uk

ABSTRACT

Multi-reference configuration interaction potential energy curves (PECs) and spin–orbit couplings for the X $^2\Pi$, A $^2\Sigma^+$, 1 $^2\Sigma^-$, 1 $^4\Sigma^-$, and 1 $^4\Pi$ states of OH are computed and refined against empirical energy levels and transitions to produce a spectroscopic model. Predissociation lifetimes are determined by discretizing continuum states in the variational method nuclear motion calculation by restricting the calculation to a finite range of internuclear separations. Varying this range gives a series of avoided crossings between quasi-bound states associated with the A $^2\Sigma^+$ and continuum states, from which predissociation lifetimes are extracted. 424 quasi-bound A $^2\Sigma^+$ state rovibronic energy levels are analyzed, and 374 predissociation lifetimes are produced, offering good coverage of the predissociation region. Agreement with measured lifetimes is satisfactory, and a majority of computed results were within experimental uncertainty. A previously unreported A $^2\Sigma^+$ state predissociation channel that goes via X $^2\Pi$ is identified in the calculations. A Python package, BINSLT, produced to calculate predissociation lifetimes, associated line broadening parameters, and lifetime uncertainties is made available. The PECs and other curves from this work will be used to produce a rovibronic ExoMol line list and temperature-dependent photodissociation cross sections for the hydroxyl radical.

I. INTRODUCTION

The hydroxyl radical OH is of significance in a diverse set of physical systems and as such has extensively been studied. OH is of high importance due to its presence in combustion, atmospheric and interstellar chemistry, and as a key constituent of the earth's atmosphere.[1–7] Furthermore, OH has recently been detected in the atmosphere of ultra-hot Jupiters WASP-76b and WASP-33b.[8,9] The many high resolution spectroscopy studies on OH have recently been comprehensively reviewed by Furtenbacher *et al.*[10] as part of their MARVEL (measured active rotation energy level) study. The *ab initio* electronic structure and predissociation dynamics of OH have been of interest for many years. Much of the early theoretical work was done by Langhoff, van Dishoeck, Dalgarno, Bauschlicher, and Wetmore,[11–15] these studies have seen extensive use in other theoretical studies.[16–24] Further *ab initio* studies have been completed more recently with more computational power and larger basis sets.[16,25–28] We particularly highlight the work of van der Loo and Groenenboom,[25] which provided a starting point for this study.

Despite the need for high-accuracy potential energy curves and coupling curves, the angular momentum coupling curves do not seem to have been reported. Angular momentum coupling is responsible for the Λ-doubling in the ground X $^2\Pi$ electronic state energy levels[29] and is required for accurate modeling of the e/f parity splittings in both X $^2\Pi$ and A $^2\Sigma^+$ states. This splitting has been reported to be anomalously high at ultra-cold temperatures;[30] hence, the angular momentum coupling between the X $^2\Pi$ state and the first electronic excited state, A $^2\Sigma^+$, should also be of interest to ultra-cold physics experiments. The effect of predissociation of the A $^2\Sigma^+$ energy levels caused by a spin–orbit interaction with repulsive (unbound) electronic states 1 $^2\Sigma^-$, 1 $^4\Sigma^-$ and 1 $^4\Pi$ is investigated. Predissociation is one of the main sources of line broadening in the A–X rovibronic transitions and has extensively been studied both

experimentally and theoretically, for which lifetimes, line positions, linewidths, rates, and branching ratios have been reported.[17–24,31–38] A summary of available lifetime data is given in Table IV. In Sec. II, details of the electronic structure calculations and spectroscopic model refinement procedure are presented. The method used to compute the predissociation lifetime is based on the use of variational bound-state nuclear-motion program DUO.[39] Section III discusses how DUO is used to study predissociation; a fuller discussion of this method will be presented in a paper,[40] henceforth referred to as Paper I. Section V presents the final spectroscopic model and compares our calculated lifetimes with their literature counterparts. A summary of the findings and proposed future work is presented in Sec. VI.

II. METHODS: *AB INITIO*

The aim of this study is to produce a complete set of predissociation lifetimes for the A $^2\Sigma^+$ state in the OH radical. An accurate spectroscopic model is needed to perform lifetime calculations. To produce this model, a high level of theory was employed to calculate *ab initio* potential energy curves (PECs) and coupling curves for the X $^2\Pi$, A $^2\Sigma^+$, and dissociative 1 ($^2\Sigma^-$, $^4\Sigma^-$, $^4\Pi$) states; see Fig. 1. These are refined against experimental values in Sec. III B.

A. *Ab initio* electronic structure calculations

The initial potential energy curves (PECs), spin–orbit coupling curves (SOCs), and angular momentum coupling curves (AMCs) were computed using the MOLPRO quantum chemistry program.[41–43] Following van der Loo and Groenenboom,[25] optimal molecular orbitals were computed using carefully selected combinations of state-averaged complete active space self-consistent field (SA-CASSCF)[44] calculations, details of which are given in Table I. These orbitals provide the input to multi-reference configuration interaction (MRCI) calculations, which included a Davidson correction[45] to the energies. The final results were computed using an aug-cc-pV6Z basis set. The calculations were performed over internuclear distances ranging from 1 to 10 a_0 with a greater density of points around the equilibrium bond length. We ensured that no $^2\Delta$ states were obfuscating the presence of the desired $^2\Sigma^\pm$ states by calculating PECs for both A_1 and A_2 irreducible representations of C_{2v} and selecting the appropriate symmetries. There are two linearly independent spin components in the $^4\Pi$ state giving rise to the same value of $|\Omega| = \frac{1}{2}$: $|1'\ ^4\Pi\rangle \rightarrow \Lambda = -1, \Sigma = \frac{3}{2}$ and $|1\ ^4\Pi\rangle \rightarrow \Lambda = 1, \Sigma = -\frac{1}{2}$.

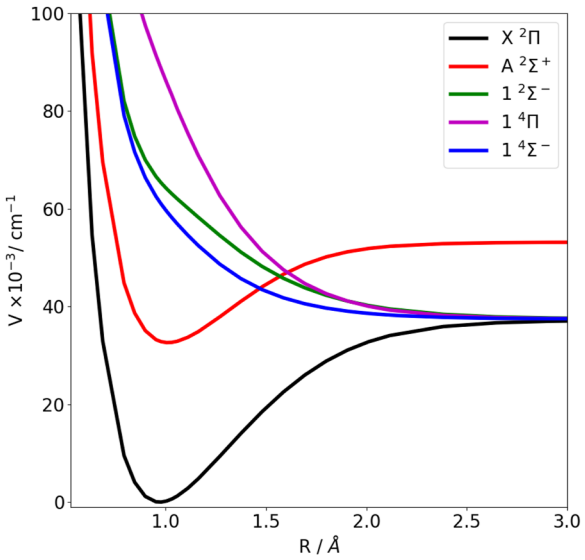

FIG. 1. *Ab initio* potential energy curves for OH as computed in MOLPRO.

TABLE I. Summary of *ab initio* electronic structure calculation details. All calculations use the aug-cc-pV6Z basis set with the first σ orbital closed. The orbitals correspond to the point group symmetry C_{2v}.

Curve	SA-CASSCF	Space
	PECs	
X $^2\Pi$	X $^2\Pi_x$, X $^2\Pi_y$	$5\sigma2\pi$
A $^2\Sigma^+$, 1 $^2\Sigma^-$	A $^2\Sigma^+$, 1 $^2\Sigma^-$	$5\sigma2\pi$
1 $^4\Sigma^-$	A $^2\Sigma^+$, 1 $^2\Sigma^-$, 1 $^4\Sigma^-$	$5\sigma2\pi$
1 $^4\Pi$	1 $^4\Pi_x$, 1 $^4\Pi_y$, A $^2\Sigma^+$	$6\sigma2\pi$
	Coupling curves	
$\langle$X $^2\Pi\|\hat{H}_{SO}\|$A $^2\Sigma^+\rangle$	X $^2\Pi_x$, X $^2\Pi_y$, A $^2\Sigma^+$	$5\sigma2\pi$
$\langle$X $^2\Pi\|\hat{L}_x\|$A $^2\Sigma^+\rangle$	X $^2\Pi_x$, X $^2\Pi_y$, A $^2\Sigma^+$	$5\sigma2\pi$
$\langle$X $^2\Pi\|\hat{H}_{SO}\|$X $^2\Pi\rangle$	X $^2\Pi_x$, X $^2\Pi_y$	$5\sigma2\pi$
$\langle$A $^2\Sigma^+|\hat{H}_{SO}|$1 $^2\Sigma^-\rangle$	A $^2\Sigma^+$, 1 $^2\Sigma^-$	$5\sigma2\pi$
$\langle$A $^2\Sigma^+|\hat{H}_{SO}|$1 $^4\Sigma^-\rangle$	A $^2\Sigma^+$, 1 $^2\Sigma^-$, 1 $^4\Sigma^-$	$5\sigma2\pi$
$\langle$A $^2\Sigma^+|\hat{H}_{SO}|$1 $^4\Pi\rangle$	1 $^4\Pi_x$, 1 $^4\Pi_y$, A $^2\Sigma^+$	$6\sigma2\pi$

The spin–orbit coupling between the A $^2\Sigma^+$ and 1 $^4\Pi$ states has the following relationship:

$$\langle 1\ ^4\Pi|\hat{H}_{SO}|A\ ^2\Sigma^+\rangle = -\sqrt{3}\langle 1'\ ^4\Pi|\hat{H}_{SO}|A\ ^2\Sigma^+\rangle, \quad (1)$$

which is derived from the application of the Wigner–Eckart theorem.[16,28] In DUO, for spin–orbit matrix elements, it is sufficient to specify only one of these combinations with the correct Λ and Σ; the other is generated using the Wigner–Eckart theorem. Here, we select 1 $^4\Pi$, where $\Sigma = -\frac{1}{2}$, $\Lambda = 1$ as is done in Parlant and Yarkony.[28] One should note it does not matter which coupling is chosen, as long as the correct Λ, Σ combination is given in Duo. MOLPRO produces coupling curves and dipoles with an arbitrary phase factor of ±1 or $\pm i$, which is not guaranteed consistent between geometries. This uncertainty in phase leads to discontinuities in the curves and hence requires post-processing. Within an MRCI calculation informed by a set of SA-CASSCF orbitals, the phase may not be consistent between geometries; however, it is consistent over all curves computed with those orbitals for a given geometry; any discontinuities will appear in the same places for all curves.[46] The coupling curves in this study, however, were not all computed with one set of orbitals and, instead, were split up as shown in the SA-CASSCF column of Table I. Inter-SA-CASSCF phase consistency was ensured by first smoothing all curves with an arbitrary

global phase and comparing to a set of reference curves. These were produced by performing an aug-cc-pVTZ calculation with all states present in the SA-CASSCF, ensuring phase consistency between all relevant curves. The visual representations of these curves are shown in Figs. 1–3.

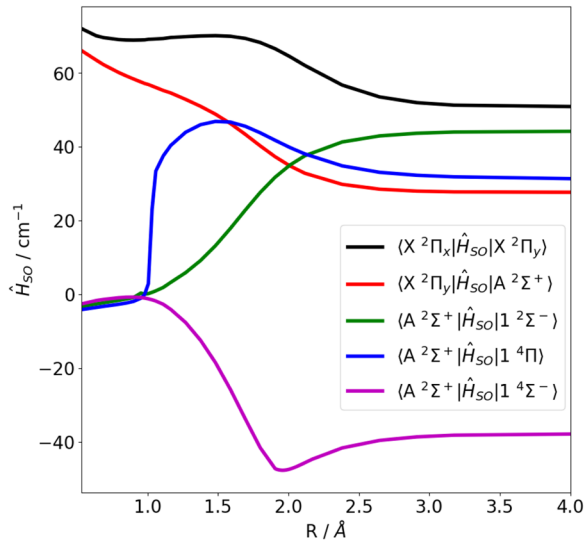

FIG. 2. Diagonal and off-diagonal *ab initio* spin–orbit coupling curves of OH as computed in MOLPRO. The curves here also have an associated factor of $\pm i$.

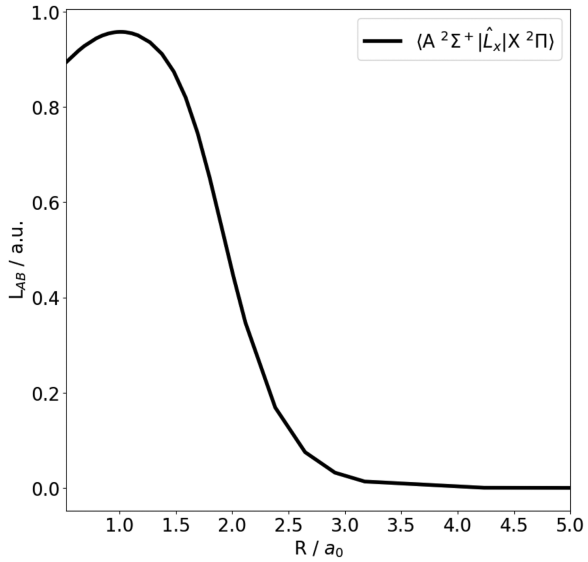

FIG. 3. *Ab initio* L-uncoupling matrix elements for OH as computed in MOLPRO. In the Cartesian coordinate system, there is a factor of $\pm i$.

III. METHODS: HYDROXYL SPECTROSCOPIC MODEL

A. Global parameters

The curves produced above provide an input to the nuclear motion code DUO,[47] an open-source Fortran 2009 program, which provides variational solutions to the coupled rovibronic Schrödinger equations for a general open-shell diatomic molecule. Rovibronic energy levels and transitions are evaluated for the mutually perturbed X $^2\Pi$ and A $^2\Sigma^+$ states. However, the *ab initio* curves are insufficient for accurate reproduction and extrapolation of energy levels for this system despite the high level of *ab initio* theory employed.

A number of global parameters need to be established before running a DUO calculation; they are as follows: the size of vibrational basis sets ($v_{\max}$) for each electronic state, the start ($r_{\min}$) and end (r_c) of the calculation box, the number of grid points, and the maximum value for J. These considerations are made to ensure converged solutions for the energy levels. The start and end of the box were set to 0.53 and 8 Å, respectively, with a grid size of 801 points. The density of rovibronic states increases with energy. States near the top end of the available vibrational basis are unstable as they are asymmetrically perturbed by local rovibronic states due to the lack of states at $v > v_{\max}$, which means that an insufficiently large $v_{\max}$ may lead to bound state solutions that may not be stable upon variation of the box size. $v_{\max}$ was selected for each electronic state iteratively. By extracting energy eigenvalues within the relevant fitting region for increasing $v_{\max}$, we can set $v_{\max}$ such that the energy levels are converged. This was found to occur when $v^X_{\max} \geq 110$ and $v^A_{\max} \geq 90$. The size of the vibrational basis sets was hence set to 110 and 90 for the X $^2\Pi$ and A $^2\Sigma^+$ states, respectively. The maximum value for J, $J_{\max}$, was set to 50.5.

B. Fitting

The PECs and coupling curves were refined by making constrained adjustments to parameters that describe them with respect to a set of observed data, which can be either empirical energy levels or transitions. These data are supplied by the recent MARVEL dataset.[10] The energy level coverage of this dataset is summarized in Table II. Curve refinement is performed in DUO by least squares fitting to this dataset.

DUO provides three types of fitting one can use: variation of parameters that describe a curve (Sec. III B 1), variation of parameters that describe a morphing function (*morphing*, see Sec. III B 2), and direct variation of individual grid points. In each case, the optimization is based on a non-linear conjugate gradient method[47] with respect to an empirical dataset.

1. Parameter variation fitting—pre-fitting

During parameter variation fitting, the curves must have some parametric form, and some initial set of parameters must be determined. For PECs, the form used in this study is the Extended Morse Oscillator (EMO),[47,48] given by

$$V_{\text{EMO}}(r) = T_e + (A_e - T_e)\left(1 - e^{-\beta(r)(r-r_e)}\right)^2, \quad (2)$$

where T_e is the potential minimum, $D_e = A_e - T_e$ is the dissociation energy relative to T_e, A_e is the dissociation asymptote, r_e is the

TABLE II. Coverage of MARVEL dataset[10] energy levels for the X $^2\Pi$ and A $^2\Sigma^+$ states of OH that have been used to refine *ab initio* PECs, SOCs, and coupling constants for the production of a spectroscopic model.

v	J_{min}	J_{max}	Number of levels
		X $^2\Pi$	
0	0.5	31.5	126
1	0.5	31.5	123
2	0.5	31.5	123
3	0.5	31.5	122
4	0.5	19.5	77
5	0.5	19.5	76
6	0.5	18.5	74
7	0.5	18.5	74
8	0.5	18.5	74
9	0.5	18.5	74
10	0.5	11.5	42
11	0.5	8.5	23
12	0.5	7.5	28
13	0.5	7.5	27
Total	0.5	31.5	1063
		A $^2\Sigma^+$	
0	0.5	31.5	64
1	0.5	28.5	58
2	0.5	19.5	40
3	0.5	26.5	54
4	0.5	19.5	40
5	0.5	7.5	15
6	0.5	8.5	17
7	0.5	7.5	16
8	0.5	9.5	19
9	0.5	8.5	17
Total	0.5	31.5	340
Grand total			1403

equilibrium bond length, and $\beta(r)$ is a distance dependent exponent coefficient defined by the expansion term with coefficients β_i with respect to the reduced coordinate ξ_p, first introduced by Šurkus *et al.*,[49] and is given by

$$\beta(r) = \sum_{i=0}^{N} \beta_i \xi_p(r)^i; \quad N = \begin{cases} N_R & \text{for } r > r_e, \\ N_L & \text{for } r \le r_e, \end{cases} \tag{3}$$

$$\xi_p(r) = \frac{r^p - r_e^p}{r^p + r_e^p}; \quad p = \begin{cases} p_R & \text{for } r > r_e, \\ p_L & \text{for } r \le r_e. \end{cases} \tag{4}$$

This parametric form is flexible in that one can specify the behavior around the equilibrium internuclear distance piece-wise using the parameters N_L, N_R, p_L, and p_R, where $N_L \le N_R$. The value of N_R, hence, defines the order of the expansion. This means that one can establish a family of potential energy curves, where the fundamental shape is determined by the set of parameters, S,

$$S = \{p_L,\ p_R,\ N_L,\ N_R\}; \quad \{p_L,\ p_R,\ N_L,\ N_R\} \in \mathbb{Z},\ N_R \ge N_L. \tag{5}$$

For a given S, one can then find P, which refines the shape to return appropriate energy levels, such that

$$P = \{\beta_i,\ r_e,\ T_e,\ D_e\}; \quad i \le N_R. \tag{6}$$

When fitting a PEC in Duo, S is fixed and hence should be carefully chosen before optimizing P. Initial parameter selection has been performed by extending the method of Mitev *et al.*[50] Given that the elements of S are integers, one cannot use a standard optimization algorithm to optimize the values and, instead, must solve the problem iteratively. The optimization of S is, therefore, initiated by establishing the set,

$$\sigma_S = \{S_0, \ldots, S_n\} \tag{7}$$

$$\equiv \{\{p_{L_0}, p_{R_0}, N_{L_0}, N_{R_0}\}, \ldots, \{p_{L_n}, p_{R_n}, N_{L_n}, N_{R_n}\}\}, \tag{8}$$

which contains n elements of the set, S, as in Eq. (5) such that

$$S_i \ne S_j \ \forall\ i, j; \quad i \ne j. \tag{9}$$

This is the set of values of p_L, p_R, N_L, and N_R over which we would like to test. The test consists of, for each S_i, finding the conjugate P_i by least-squares fitting against the *ab initio* grid points in Python (code available on ExoMol GitHub). In each case, we find the reduced χ^2 test statistic, χ^2_v, and search for S and P, which return the lowest value. These parameters are then used as a starting point for fitting the PECs against experimental data in Duo. See Table III for the σ_i parameters for the X $^2\Pi$ and A $^2\Sigma^+$ states in this study.

2. Morphing

As discussed above, morphing is another available technique for model refinement. In this case, one does not vary the curve in

TABLE III. Parameters, σ_i, that best describe *ab initio* PECs of OH as calculated in Sec. II A. Units: $[T_e]$ = cm^{-1}. $[A_e]$ = cm^{-1}. $[r_e]$ = Å. $[\beta_i]$ = Å^{-1}.

X $^2\Pi$		A $^2\Sigma^+$	
T_e	0	T_e	32 612.251 248 000
r_e	0.970 655 035	r_e	1.013 454 000
A_e	37 269.126 195 730	A_e	53 204.256 220 000
p_L	4	p_L	3
p_R	3	p_R	3
N_L	6	N_L	4
N_R	8	N_R	8
β_0	2.292 052 187	β_0	2.620 396 000
β_1	−0.019 995 181	β_1	0.169 768 000
β_2	0.198 099 686	β_2	0.465 289 000
β_3	0.231 459 916	β_3	0.552 208 000
β_4	−0.136 025 012	β_4	0.413 921 000
β_5	−0.639 517 770	β_5	−5.174 652 000
β_6	−0.277 770 706	β_6	9.999 998 000
β_7	6.274 892 232	β_7	3.333 865 000
β_8	−4.898 195 146	β_8	−9.999 764 000

question directly but, instead, varies a morphing function, $f_m(r)$, which, in turn, scales the *ab initio* curve, $f_{ai}(r)$,[51,52]

$$f_{morphed}(r) = f_{ai}(r) f_m(r). \tag{10}$$

As was done in Mitev *et al.*,[50] the *polynomial decay* morphing function was used,

$$f_m(r) = \sum_{k=0}^{N} B_k z^k (1 - \xi_p) + \xi_p B_\infty, \tag{11}$$

where

$$z(r) = (r - r_{ref}) e^{-\beta(r-r_{ref})^2 - \gamma(r-r_{ref})^4},$$

ξ_p is as in Eq. (4), B_k are variable expansion coefficients, β and γ are static coefficients typically set to 0.8 and 0.02, respectively, B_∞ is typically set to unity to preserve the asymptotic behavior of f_{ai}, N is the order of expansion, and r_{ref} is the expansion center. r_{ref} is set to the equilibrium bond length of the lower energy electronic state. When fitting Eq. (11), only the B_k parameters are floated.

3. Constraining curves

The asymptotic energy limit for all the curves in Fig. 1 was constrained by setting the value of D_e^X to the experimental value of D_0 from Joens[5] with the added offset from the zero-point energy of the X $^2\Pi$ state, E_0^X calculated in DUO, hence

$$D_e^X = D_0 + E_0^X. \tag{12}$$

The remaining curves' D_e was constrained with respect to D_e^X such that their respective atomic limit spacings match that of Kramida *et al.*[53]

C. MARVEL dataset and quantum number conventions

Furtenbacher *et al.*[10] collected 15 938 rovibronic transitions from 45 sources and produced values for 1624 empirical rovibronic energy levels for the system of electronic states, X $^2\Pi$, A $^2\Sigma^+$, B $^2\Sigma^+$, and C $^2\Sigma^+$. 12 413 and 1403 of these transitions and empirical energy levels, respectively, concern the X $^2\Pi$ and A $^2\Sigma^+$ states. Table II presents the coverage of the MARVEL energy levels used in this study.

The complete set of quantum numbers used to characterize the MARVEL energy levels are the state label (X $^2\Pi$, A $^2\Sigma^+$, 1 $^2\Sigma^-$, ...) total angular momentum, J, the vibrational quantum number, v, the rotationless parity, e/f, and the projection of the total angular momentum on the molecular axis, $\Omega = \Sigma + \Lambda$, where Σ and Λ are the projections of the spin and orbital angular momenta on the molecular axis, respectively.

In line with Hund's case (a) conventions used in DUO, the following quantum numbers are used to characterize the rovibronic states, $|J, v, \tau, \Sigma, \Lambda, \Omega, State\rangle$, where *State* is a counting number associated with the electronic states as ordered by potential minima, T_e, and τ is the state parity ± (see Tennyson *et al.*[29] for conversion between e/f and τ), which can be directly related to the MARVEL dataset.

Instead of using Hund's case (a) convention, many datasets on the rovibronic state of OH in the literature opt for the rotational quantum number N and the fine structure components, F_1 and F_2 [Hund's case (b)]. In order to correlate these data with our MARVEL dataset, their representations have been converted to the rigorous quantum labels J and e/f using the following relations.

For the A $^2\Sigma^+$ state:

$$J = \begin{cases} N + \frac{1}{2} & \text{for } F_1, \\ N - \frac{1}{2} & \text{for } F_2, \end{cases} \tag{13}$$

$$e/f = \begin{cases} f & \text{for } F_1, \\ e & \text{for } F_2. \end{cases} \tag{14}$$

These relations arise, in particular, as the A $^2\Sigma^+$ state levels are generally presented using Hund's case (b), hence the relation between J and N, Eq. (13), and due to the common approximation,

$$E_{F_1} = BN(N+1) + \frac{1}{2}\gamma N, \tag{15}$$

$$E_{F_2} = BN(N+1) - \frac{1}{2}\gamma(N+1). \tag{16}$$

Therefore, because $\gamma \ll B$,[7] where B is the rotational constant and γ is the spin-rotation constant,

$$E_{F_1} > E_{F_2} \quad \forall \quad N, J \tag{17}$$

and since the A $^2\Sigma^+$ state has only parity splitting as $\Lambda^A = 0$, the F_1 and F_2 components correspond directly to f and e parities, respectively (see Herzberg[54]).

For the X $^2\Pi$ state, the relevant Hund's case (a) approximation is

$$E_{F_1} = B[(J+S)^2 - \Lambda^2] - \frac{1}{2}(A - 2B), \tag{18}$$

$$E_{F_2} = B[(J+S)^2 - \Lambda^2] + \frac{1}{2}(A - 2B), \tag{19}$$

where A is the diagonal spin–orbit coupling. This is applied for a given parity and correlates with the following relation:[54]

$$E_{F_1} = E\left(\Omega = \frac{3}{2}\right), \tag{20}$$

$$E_{F_2} = E\left(\Omega = \frac{1}{2}\right). \tag{21}$$

The quantum number correlations for the quartet 1 $(^4\Sigma^-, ^4\Pi)$ states have not been considered here as there are no experimental data that will require transformation.

IV. METHODS: PREDISSOCIATION LIFETIMES

OH predissociation lifetimes have long been the subject of theoretical and experimental studies; a summary of the available literature data is provided in Table IV. The data provided by Heard *et al.*[34] and Spaanjaars *et al.*[35] are given as predissociation rates,

TABLE IV. Summary of predissociation lifetime data available from experimental and theoretical sources.

Reference[a]	Lifetime (ps) Min	Lifetime (ps) Max	v Min	v Max	J Min	J Max	Number of lifetimes	Data type
				Experiment				
05DePoDe[31]	17	23	4	4	0.5	7.5	8	Predissociation lifetimes
21SuZhZh[36]	14	130 000	2	4	0.5	2.5	2	Predissociation lifetimes
78BrErLy[32]	33 000	1 110 000	0	2	0.5	29.5	118	Total lifetimes
91GrFa[33]	73	500	3	3	0.5	9.5	17	Predissociation lifetimes
92HeCrJe[34]	62.89	312.50	3	3	0.5	13.5	27	Predissociation rates
97SpMeMe[35]	29	167	3	3	4.5	14.5	20	Predissociation rates
				Theory				
80SiBaLe[38]	2.95	428.16	3	9	Not J resolved		7	Predissociation lifetimes
94KaSa[18]	3.32	6895.10	1	7	Not J resolved		7	Predissociation lifetimes
99PaYa[28]	6000	9 666 000	0	4	0.5	30.5	107	Predissociation lifetimes
Grand total							313	
This work	2.1	3 600 000	0	9	0.5	35.5	374	Predissociation lifetimes

[a]Reference tags are given as YYAaBbCc, where YY is the last two digits of the publication year and AaBbCc is first two letters of (up to) first three authors' surnames in order of appearance.

and these have been inverted to return the required predissociation lifetimes. Brzozowski *et al.*[32] provides measurements of the total lifetime, which is given by

$$\tau = \frac{\tau_r \tau_p}{\tau_r + \tau_p}, \tag{22}$$

where τ_r and τ_p are the radiative and predissociative lifetimes, respectively. As these values include also the radiative lifetime, we expect our calculations to be greater than these values. This is compounded by the fact that the predissociation in the region of $v \in [0, 1, 2]$ is less dominant than in $v \geq 3$.

A novel method for the calculation of predissociation lifetimes is applied in this section. The full details of the method will be available in Paper I; however, a brief summary of the method is given below.

A. Energy resonances

An excited rovibronic state from A $^2\Sigma^+$ can predissociate via a spin–orbit interaction with a local repulsive state inducing the decay.[17,20,28,36,37]

In Fig. 4, the two green horizontal lines illustrate the unbound state energy levels retrieved from DUO calculations with different right-side box limits, r_c. Both sets of calculations are performed with the same left-side box limit $r_{\min}$. By construction, the nuclear motion wavefunctions are only finite between r_c and $r_{\min}$. The two green unbound state energy levels have the same quantum numbers $J, v, \tau, \Sigma, \Lambda, \Omega$; however, $E_{r_c=3\text{Å}}$ returns a higher term value than $E_{r_c=4\text{Å}}$. This is akin to the particle in a box, where increasing the size of the box compresses the distribution of energy levels closer to zero. Repeated calculations over varying r_c in DUO for iso-numeric continuum energy levels exhibit a relationship, where the term values decrease with r_c; this is referred to as the *energy profile* of the continuum energy level.

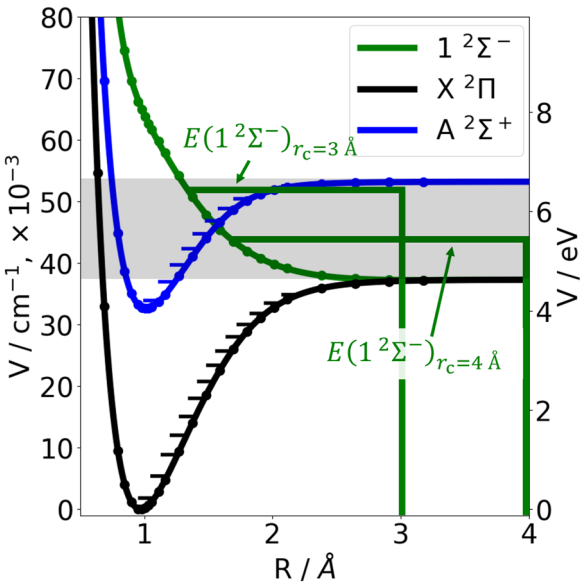

FIG. 4. A toy model of OH consisting of the X $^2\Pi$, A $^2\Sigma^+$, and 1 $^2\Sigma^-$ electronic states. The two green levels, $E(1\,^2\Sigma^-)_{r_c=3,4\ \text{Å}}$, are continuum levels in the 1 $^2\Sigma^-$ electronic state with the same quantum numbers, however, with different right-side box limits, r_c. This highlights the box size dependence of repulsive state energy levels. The shaded region covers energy levels between D_e^X and D_e^A.

The spin–orbit interaction between the 1 $^2\Sigma^-$ and A $^2\Sigma^+$ states, $\langle {}^2\Sigma^- | \xi | {}^2\Sigma^+ \rangle$, hence displaces the A $^2\Sigma^+$ state levels, which would

otherwise be stable under variation of r_c. This *induced energy profile* allows us to study the predissociation characteristics of the quasi-bound A $^2\Sigma^+$ state levels.

The energy levels of interest for this study are found in the shaded region of Fig. 4. This covers 424 rovibronic energy levels in the A $^2\Sigma^+$ state.

The quantum number coverage for the relevant energy levels is presented in Table V. Being above the first dissociation channel (D_e^X), each of these levels is quasi-bound and metastable with an associated characteristic lifetime, which we compute here. As discussed below, not all levels in the range had calculable predissociation lifetimes as per the method in Paper I, especially for levels with energy close to D_e^X.

Since repulsive electronic states have an infinitely dense set of continuum states, the position of the predissociating state, $|\mathrm{A}\ ^2\Sigma^+, Q\rangle$, where Q is the complete set of quantum numbers, $\{J, v, \tau\}$, has an uncertainty in the energy caused by the Pauli exclusion principle. This infinite set of states cannot be recovered using bound state methods for solving the Schrödinger equation for $r_c \to \infty$, such as used by Duo, although more expensive scattering methods can be employed using Duo just for the inner region.[55]

Here, we approximate the continuum behavior by discretizing the continuum[56] and adapting the stabilization method[57–59] to characterize the quasi-bound states. In this method, infinite potential walls are assumed at the box limits $r_{\min}$ and r_c, leading to bound-like rovibronic solutions even for continuum or quasi-bound states. By changing the position of the right-side wall r_c, different continuum state term values can be generated and the uncertainty of the position of the quasi-bound states can be quantified as follows.

For a given box size defined by $r_c - r_{\min}$ with an infinite potential wall, one can compute the term values $\tilde{E}_{|\mathrm{A},Q\rangle}|_{r_c}$ of the given set of quasi-bound, metastable states $\{|\mathrm{A}\ ^2\Sigma^+, Q\rangle\}$. By varying r_c, one can then establish a dependence of $E_{|\mathrm{A},Q\rangle}$ on r_c. In this study, r_c was varied between $r_c = 8$ and 8.999 Å with the uniform spacing of 999 values ($\delta r_c = 0.001$ Å). This was done by repeating the Duo calculations while varying the right-side limit, r_c (see Sec. III A), and extracting the eigenenergies at each step. The number of Duo sinc-DVR (discrete variable representation)[60] grid points was increased as the box size was increased to maintain a uniform grid. Out of 999 runs, about 20 calculations failed, but these were simply ignored.

Figures 5 and 6 illustrate the box-size dependence for two A $^2\Sigma^+$ quasi-bound states of OH, $|\mathrm{A}\ ^2\Sigma^+, J = 0.5, v = 4, e\rangle$ and $|\mathrm{A}\ ^2\Sigma^+, J = 0.5, v = 2, e\rangle$, showing their "stabilization" character. The behavior is seen to be periodic with discontinuities at visually regular intervals and a central energy region in the middle. The typical resonance-like shapes are due to the interactions with continuum states. The discontinuities occur at the geometries where a crossing continuum energy level goes from pushing the quasi-bound level down to pushing it up and provide the energy level resonances from which we can calculate lifetimes. The line broadening parameter, Γ, and hence the lifetime of the state, $\tau \propto 1/\Gamma$, are associated with the widths of these resonances.

The interaction between A $^2\Sigma^+$ and the three continuum states 1 $^2\Sigma^-$, 1 $^4\Sigma^-$, 1 $^4\Pi$ are through the corresponding spin–orbit couplings from Fig. 2. There are several structures visible in Fig. 5, the asymptotes with the large wings and the asymptotes with the small wings. These substructures are caused by spin–orbit interactions with different electronic states, 1 $^2\Sigma^-$, 1 $^4\Sigma^-$, or 1 $^4\Pi$. The individual contributions can be resolved by performing calculations with only one of the three repulsive states and associated spin–orbit couplings present at a time, as illustrated in Fig. 6 for the $|\mathrm{A}\ ^2\Sigma^+, J = 0.5, v = 2, e\rangle$ state (this state has been chosen for its simplicity). It shows that all three states contribute to the minor asymptotic wings, but only the 1 $^4\Sigma^-$ state corresponds to the major wings. This makes the 1 $^4\Sigma^-$ state a bigger contributor to the predissociative decay for this particular state (due to a greater effect on the overall broadening), which is corroborated by the branching ratios reported by Li and Zhang,[37] who show that the 1 $^4\Sigma^-$ state is the primary branch.

For energy levels above D_e^X, X $^2\Pi$ state rovibronic levels become unbound and contribute to the perturbation of the A $^2\Sigma^+$ state level energies and hence provide an additional avenue for predissociation

TABLE V. Quantum number coverage for quasi-bound A $^2\Sigma^+$ state rovibronic levels.

v	$J_{\min}$	$J_{\max}$	Number of levels	Number of lifetimes[a]
0	13.5	35.5	44	21
1	2.5	33.5	62	35
2	0.5	31.5	63	63
3	0.5	28.5	57	57
4	0.5	25.5	51	51
5	0.5	22.5	45	45
6	0.5	19.5	39	39
7	0.5	15.5	31	31
8	0.5	11.5	23	23
9	0.5	4.5	9	9
Total			424	374

[a]Number of levels for which a lifetime calculation is meaningful.

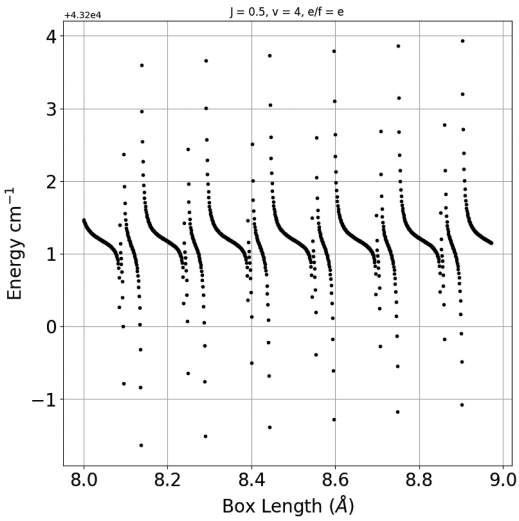

FIG. 5. Term value of the $|\mathrm{A}\ ^2\Sigma^+, J = 0.5, v = 4, e\rangle$ state as a function of the box length of the calculation in Duo; the variation of the energy is induced by crossings with energy levels in the repulsive states 1 $^2\Sigma^-$, 1 $^4\Sigma^-$, and 1 $^4\Pi$.

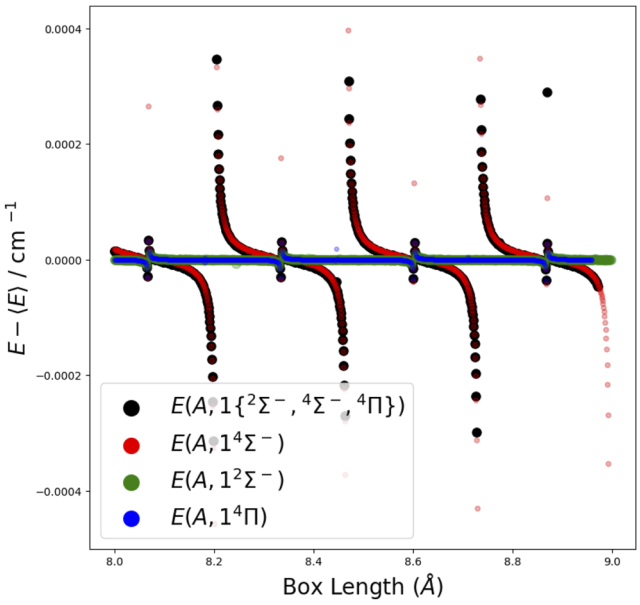

FIG. 6. Term value of the $|A\,^2\Sigma^+, J = 0.5, v = 2, e\rangle$ state as a function of the box length of the calculation in Duo. The different colors correspond to different spin–orbit contributions.

through the ground electronic state; see Fig. 7. The effect of predissociation through the X $^2\Pi$ state is small and does not appear to have previously been reported. This effect cannot be isolated in our calculations, however, as removing the spin–orbit coupling between the X $^2\Pi$ and the A $^2\Sigma^+$ states shifts the energy levels too strongly (hundreds of cm^{-1}) to be comparable.

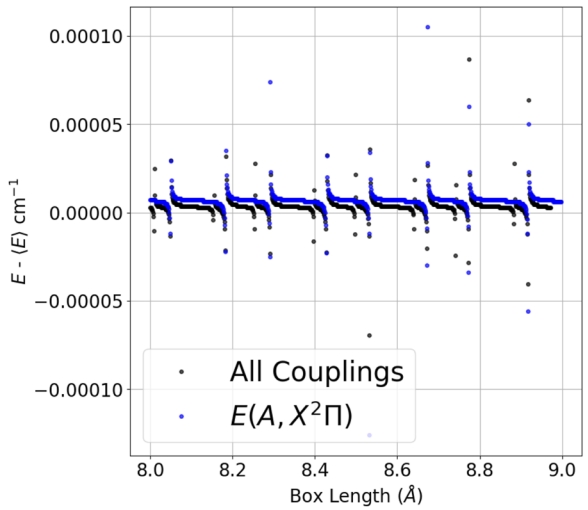

FIG. 7. Term value of the $|A\,^2\Sigma^+, J = 13.5, v = 1, f\rangle$ state as a function of the box length for a Duo calculation including the X $^2\Pi$ and A $^2\Sigma^+$ states only. The blue markers represent a shift in energy induced by the spin–orbit coupling between the X $^2\Pi$ and A $^2\Sigma^+$ states on the A $^2\Sigma^+$ state level.

B. Statistical treatment

To calculate the predissociation lifetime from the above results, one calculates the integral normalized histogram of the energy data points centered around the mean $(E - \langle E\rangle)$; see Fig. 8 for an example. The binning of the histogram and the training of the Lorentzian parameters are non-trivial and are discussed in Paper I.

The probability function describing the system's energy profile has the Lorentzian distribution,[19]

$$L(\tilde{E}; \tilde{E}_0, \Gamma) = \frac{\frac{1}{\pi}\left(\frac{1}{2}\Gamma\right)}{(\tilde{E} - \tilde{E}_0)^2 + \left(\frac{1}{2}\Gamma\right)^2}, \tag{23}$$

where $\tilde{E}_0$ is the peak position of the Lorentzian and Γ is the full width at half maximum (line broadening parameter, in cm^{-1}). The parameters $\{\tilde{E}_0, \Gamma\}$ can be trained to best represent the histogram in Fig. 8; then, the parameter Γ is inverted via the following relationship:

$$\tau_p = \frac{1}{2\pi c\Gamma}, \tag{24}$$

where c is the speed of light in cm s^{-1}.

There is an associated uncertainty to the fitting of the Lorentzian profile, and this is discussed in Sec. IV 3. The Python package, BINSLT was written to perform these calculations; it is available for download from https://github.com/exomol.

A visualization of the Lorentzian-distributed energy histogram is shown in Fig. 8, where it is superimposed with the corresponding induced energy profile for the $|A\,^2\Sigma^+, J = 0.5, v = 4, e\rangle$ state.

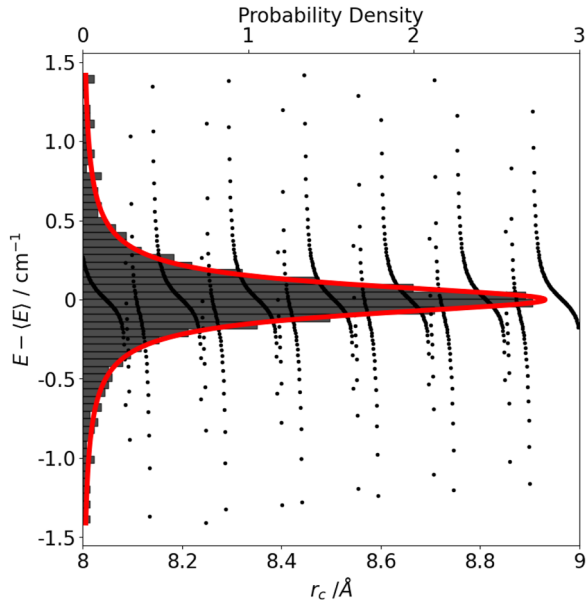

FIG. 8. Plot of the energy against box length with the fitted histogram of energy points for the $|A\,^2\Sigma^+, J = 0.5, v = 4, e\rangle$ state.

C. Uncertainty estimation

The largest uncertainties arise in states with long predissociation lifetimes. Here, we will consider only the lifetimes which are shorter than the radiative lifetimes. As discussed in Paper I, the uncertainty is made up for four components, which are assumed independent and systematic and so are added to produce a final uncertainty Δ_τ,

$$\Delta_\tau = \Delta_M + \Delta_R + \Delta_B + \Delta_C, \tag{25}$$

where Δ_M is the uncertainty from convergence, which is defined as $1 - M$, where M is the convergence level of the lifetime for a given state. This is typically the largest uncertainty, and in cases of long lifetimes ($\tau_p > 10^5$ ps), this can be as high as 20%. For lifetimes between 10^4 and 10^5 ps, Δ_M is evaluated at 10%, and for lifetimes shorter than 10^4 ps, this is found to be 5%.

Δ_R and Δ_B are the uncertainties from the positions of the repulsive and bound states' energy levels. Δ_B is very difficult to measure directly, as it requires that the energy level positions of the bound states can be controlled with high precision in order to establish a relationship between the energy offset and the lifetime. This is, at the moment, infeasible. This has been estimated, however, by probing the effect the repulsive energy level positions have on the lifetimes. The asymptotic energy of the continuum states goes to the O(^{3}P) level, the same as the X $^2\Pi$ state. $D_e(X)$ has experimentally been measured to an uncertainty of 10 cm^{-1} by Joens[5] (see Sec. III B 3). Our continuum curves were shifted down by 20 cm^{-1}, and the lifetimes for the predissociative states with $J \in [0.5, 1.5]$ were re-computed and compared to the original model. This gives a conservative estimate on the uncertainty due to the position of the continuum curves, Δ_R of about 5%. The A $^2\Sigma^+$ state energy level position induced uncertainty, Δ_B, is hence also estimated at 5%.

Δ_C is the uncertainty of the numerical procedure excluding the problem of convergence. This is evaluated *in situ* for each state and has an average value over all states of ~2% in the case of OH. These uncertainties are distributed exponentially as is seen in Fig. 9.

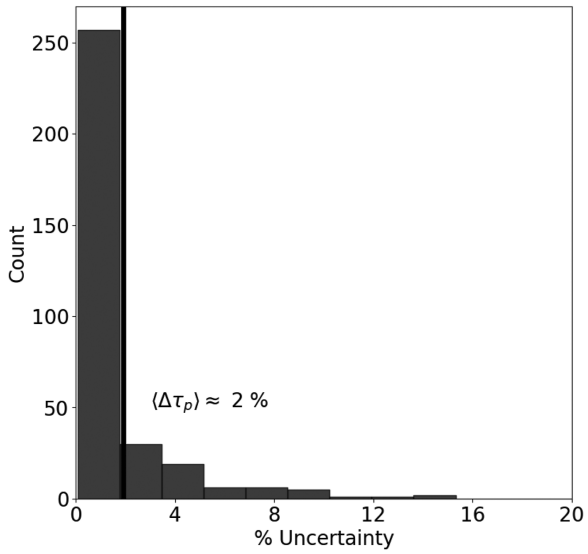

FIG. 9. Distribution of percentage uncertainties in the lifetime induced by the computational procedure.

TABLE VI. Rules for attributing uncertainties for predissociation lifetimes calculated using the stabilization method for OH.

Quantity	Value		
Lifetime range (ps)	$[0, 10^4]$	$[10^4, 10^5]$	$[10^5, 10^7]$
Average uncertainty (%)	$15 + \Delta_C$	$20 + \Delta_C$	$30 + \Delta_C$

The lifetimes supplied in the supplementary material have been fully treated as in the methods described above and, more completely, in Paper I. Table VI gives a summary of the average uncertainties over different ranges of lifetimes in ps.

V. RESULTS

A. Spectroscopic model parameters

Refinement of the curves representing the coupled model of the two states X $^2\Pi$ and A $^2\Sigma^+$ in Duo was performed by floating the parameters $r_e(X, A)$, $T_e(A)$, $\beta_i(X, A)$ (PECs) and B_k (spin–orbit and L-uncoupling curves).

Couplings to higher electronic states have not been considered for the sake of simplicity in the model. Furthermore, couplings to repulsive electronic states for refinement of bound state energy levels have not been considered either. This has been done due to computational limitations as the box size of the calculation becomes an independent variable for the energy levels; see discussions above.

Along with the adjusted PECs and the *morphed* coupling curves, three more *empirical*, diagonal curves have been introduced to account for the aforementioned missing couplings.[29] These are the spin-rotation, $\gamma(X, A)$, the Λ-doubling $\alpha_{p2q}(X)$ and $q(X)$,[61] and the Born–Oppenheimer breakdown (BOB) radial property function.[62] The inclusion of such factors was necessary to refine the energy level reproduction without requiring the introduction of further electronic states or off-diagonal couplings. The Šurkus polynomial expansion function, $C(r)$ [see Eq. (26)], has been used as the parametric representation,[63]

$$C(r) = T_e + (1 - \xi_p)\sum_{i\geq 0} B_i \xi_p^i + \xi_p B_\infty, \tag{26}$$

where ξ_p is the reduced coordinate in Eq. (4). The parameters B_i and B_∞ are floated.

The dissociation limits, $D_e(X, A)$, were fixed to the values $D_e = D_0 + \text{ZPE}$, where the zero point energy of the ground state was extracted from the Duo calculation and found to be ~1918 cm^{-1}, $D_0(X)$ was measured by Joens[5] to ±10 cm^{-1} $D_e = D_0 + \text{ZPE}$, while $D_e(A)$ was estimated by adding the difference in energy between the O(^{3}P) and O(^{1}D) atomic levels using values from the NIST Online Database.[53]

In Duo, one can fit the spectroscopic model both against datasets of energy levels and of transitions in Duo. The process taken in this work was to fit it against the experimentally derived (MARVEL) energy levels by Furtenbacher *et al.*[10]

A summary of fitted parameters is available in Tables VII–IX, and a summary of uncertainties and rms values is available in Table X. The Duo input file is given in the supplementary material.

TABLE VII. Summary of the PEC parameters obtained from least squares fitting the X $^2\Pi$ and A $^2\Sigma^+$ states of OH to MARVEL energy levels from Furtenbacher *et al.*[10] in Duo.[47] All the figures are kept for the sake of preserving accuracy and reproducibility.

Parameter	X $^2\Pi$	A $^2\Sigma^+$
T_e	0	32 663.976 309 068 300
r_e	0.970 020 962 666	1.005 285 998 312
A_e	37 501.792 600 000 000	53 369.654 600 000 000
p_L	4	3
p_L	3	3
N_L	6	4
N_R	9	8
β_0	2.287 411 349 533	2.625 193 503 966
β_1	−0.008 481 205 971	0.137 874 402 944
β_2	0.138 199 166 549	0.280 685 923 916
β_3	−0.066 491 288 959	0.687 146 152 607
β_4	0.249 817 374 269	1.374 869 049 258
β_5	1.855 331 479 551	−2.136 036 385 410
β_6	2.083 877 071 440	−14.858 091 727 498
β_7	−21.177 505 781 638	45.312 091 462 135
β_8	34.392 719 961 367	−32.477 114 187 491
β_9	−16.859 334 102 231	

B. Predissociation lifetimes

BINSLT was used to compute the predissociation lifetimes of 374 quasi-bound A $^2\Sigma^+$ rovibronic states with follow-up processing completed as further described in Paper I. Fifty out of the allowed 424 states could not be processed as their energy profiles were too narrow and had insufficient resolution to compute Γ_p.

A comparison with the lifetimes available in the literature (experiment and theory) and this work is illustrated in Fig. 10, where the lifetime values are plotted as a function of J. The corresponding J-averaged percentage errors and their standard deviations are given in Table XI. A full tabulation of these data is available in the supplementary material for reference.

Table XI shows that there is a satisfactory agreement between the lifetimes presented here and experiment; there is particularly good agreement for the cases where $v = 3, 4$; see Fig. 10. In these cases, most results agreed within uncertainty (51/73 cases), and in regions where they did not agree, the mean percentage real difference in this region is 15%. The percentage real difference, ${}^{\mathrm{R}}\Delta_{\%}$, and the percentage difference, $\Delta_{\%}$, here are defined as

$$D = \frac{|\Delta| - (\delta_{\mathrm{calc}} + \delta_{\mathrm{lit}})}{\tau_{\mathrm{lit}}}, \tag{27}$$

$${}^{\mathrm{R}}\Delta_{\%} = \begin{cases} D & \text{for } D > 0, \\ 0, & \text{otherwise}, \end{cases} \tag{28}$$

$$\Delta_{\%} = \frac{\tau_{\mathrm{lit}} - \tau_{\mathrm{calc}}}{\tau_{\mathrm{lit}}} \equiv \frac{\Delta}{\tau_{\mathrm{lit}}}, \tag{29}$$

where τ_{lit} and τ_{calc} are the literature and calculated predissociation lifetimes, respectively, Δ is the difference in those values, and δ_{lit} and δ_{calc} are the uncertainties quoted in the literature and calculated values, respectively.

TABLE VIII. Summary of the *morphing* parameters obtained from least squares fitting the X $^2\Pi$ and A $^2\Sigma^+$ states of OH to MARVEL energy levels and transitions from Furtenbacher *et al.*[10] in Duo.[47]

Parameter	ξ_X	ξ_{XA}	L_{XA}
r_e	0.970 655 034 638	0.970 655 034 638	0.970 444 387 498 1
β	0.8	0.8	0.8
γ	0.02	0.02	0.02
p	6	6	2
B_0	1.008 496 273 609	0.675 170 320 954	0.772 527 250 694
B_1	−0.504 517 931 107	−0.799 178 556 532	−0.649 959 182 912
B_2	0.127 429 582 028	−2.036 097 977 961	−0.712 564 567 820
B_∞	1.000 000 000	1.000 000 000	1.000 000 000

TABLE IX. Summary of the empirical parameters obtained from least squares fitting the X $^2\Pi$ and A $^2\Sigma^+$ states of OH to MARVEL energy levels and transitions from Furtenbacher *et al.*[10] in Duo.[47]

	BOB(A $^2\Sigma^+$)	γ_X	γ_A	α_{p2q}	q
r_e (Å)	0.969 785 542 585	0.969 785 542 585	0.969 785 542 585	0.969 785 542 585	0.969 785 542 585
p	2	2	2	2	2
N	3	3	3	3	3
B_0 (Å^{-1})	−0.013 387 427 200	−0.082 615 835 520	0.107 579 056 717	0.081 298 271 720	−0.015 657 399 328
B_∞ (Å^{-1})	−0.000 897 768 443	0.029 822 159 900	0.019 259 293 154	−0.116 865 046 681	0.016 057 094 058

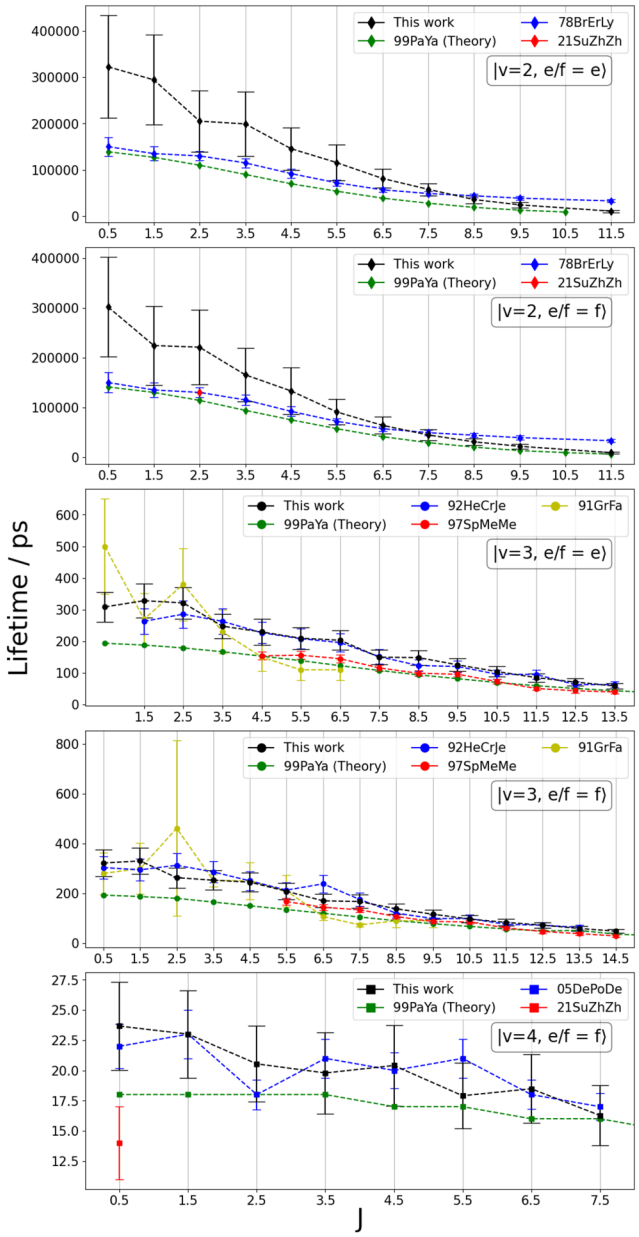

FIG. 10. Predissociation lifetimes as calculated in this work compared to experimental values from 05DePoDe,[31] 78BrErly,[32] 91GrFa,[33] 92HeCrJe,[34] 97SpMeMe,[35] and 21SuZhZh[36] and theoretical values from 99PaYa.[28]

The noticeable exceptions to this are the lifetimes for $v \in [0, 1, 2]$ from Brzozowski *et al.*[32] The experimental values in question here are total lifetimes rather than predissociation lifetimes. For $v < 2$, radiative decay is the dominant source of broadening; hence, the lifetimes of Brzozowski *et al.*[32] measurements should underestimate the predissociation lifetime. For $v = 2$, predissociation is dominant; however, radiative decay appears to be significant in the low J region (<6.5).

TABLE X. Summary of the energy rms values, in cm^{-1}, obtained from least squares fitting the X $^2\Pi$ and A $^2\Sigma^+$ states of OH to MARVEL transitions from Furtenbacher *et al.*[10] in Duo.[47]

v	rms_X	rms_A
0	0.08	0.07
1	0.09	0.19
2	0.15	1.05
3	0.08	0.76
4	0.12	0.61
5	0.06	1.96
6	0.11	3.23
7	0.14	4.70
8	0.08	1.64
9	0.25	4.58
10	0.25	
11	0.70	
12	1.34	
13	1.13	
Whole state	0.33	1.79

TABLE XI. Summary of comparison between predissociation lifetimes as calculated in this work and available literature values. Differences are averaged over J for a given v. Only rotationally resolved literature lifetimes are compared here (see Table IV). Full comparison dataset is provided in the supplementary material. The columns are as follows: Type = experiment or theory. Ref = reference. v = vibrational quantum number. $\langle\Delta_{\%}\rangle$ = average percentage difference. Number = number of J resolved levels. C_A = number of levels whose lifetimes agree within uncertainty. $\langle {}^R\Delta_{\%}\rangle$ = average ${}^R\Delta_{\%}$ for values that do not agree within uncertainty.

Type	Ref.	v	$\langle\Delta_{\%}\rangle$	Number	C_A	$\langle {}^R\Delta_{\%}\rangle$
Expt.	05DePoDe[31]	4	−0.2	8	8	0.0
	21SuZhZh[36]	2	−70.0	1	0	12.2
		4	−69.1	1	0	21.7
	78BrErLy[32]	0	−72.6	9	5	77.0
		1	−137.5	6	3	123.1
		2	−28.5	22	12	24.2
	91GrFa[33]	3	−26.7	17	13	39.5
	92HeCrJe[34]	3	−2.0	27	26	2.1
	97SpMeMe[35]	3	−40.5	20	4	11.7
Theory	99PaYa[28]	0	−76.7	11	4	34.9
		1	−77.1	9	3	27.0
		2	−87.2	23	0	33.0
		3	−48.0	35	1	25.6
		4	−15.3	21	12	6.1

One can consider the individual widths of the radiative and predissociative components, $\Gamma_{r,p}$, and that the total width is $\Gamma = \Gamma_r + \Gamma_p$ and extract the dominance of the radiative decay, R_D, such that

$$R_D = \frac{\Gamma_r}{\Gamma}. \quad (30)$$

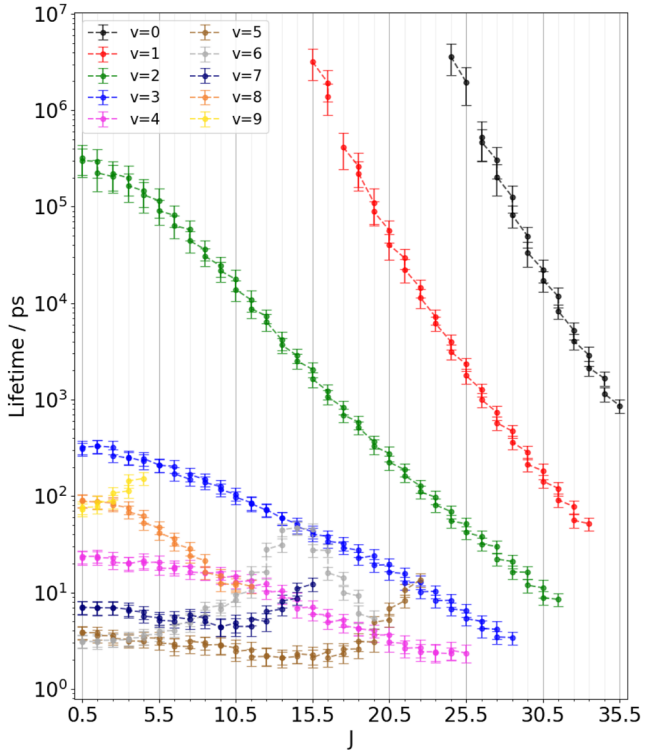

FIG. 11. Statistical predissociation lifetimes calculated for quasi-bound rovibronic A $^2\Sigma^+$ state levels using code BINSLT from Paper I. Lifetimes presented against J for varying v.

From our calculations, we compute R_D and estimate the predissociation lifetime of Brzozowski *et al.*[32] through the following relation:

$$\tau_p = \frac{\tau}{1 - R_D}, \tag{31}$$

and from this, we are able to recover agreement within uncertainty with Brzozowski *et al.*[32]

A visualization of the computed predissociation lifetimes from this work against total angular momentum J is presented in Fig. 11. For $v > 4$, we find that lifetimes behave less predictably, wherein they do not decrease monotonically. The cause of this has not yet been identified with certainty; however, we expect this to be due to the quasi-bound energy level falling outside of the main crossing region.

In $v = 6$, we see that the lifetime increases and then falls again at $J = 15.5$. OH has a high rotational constant of around 20 cm^{-1}, and in the high J limit, there is an induced rotational barrier. This modifies the potential and introduces a further source of predissociation. In this limit, it would be expected that this added source of predissociation would lower the lifetime. This type of predissociation is particularly dominant in AlH and warrants further study.[64]

VI. CONCLUSION AND DISCUSSION

A spectroscopic model of OH from *ab initio* potential energy curves and coupling curves and empirical coupling curves that are refined against latest empirical energies[10] is produced using the nuclear motion code DUO. This spectroscopic model will be extended to include the $B^2\Sigma^+$ and $C^2\Sigma^+$ states and combined with *ab initio* dipole moment curves to produce a line list and photoabsorption cross section for hot OH as part of the ExoMol project. This line list will include predissociation lifetimes using the newly extended ExoMol data structure;[65] broadening effects due to predissociation have been shown to be important in analyzing astronomical spectra.[64]

424 quasi-bound A $^2\Sigma^+$ state rovibronic levels are processed using the method of Paper I to calculate a set of 374 predissociation lifetimes, τ_p. This method has produced a set of predissociation lifetimes from first principles with uncertainties and provides a satisfactory level of agreement with experimental values. The method used in this paper allows for completeness over all levels considered in a spectroscopic model and is applicable to other systems.

According to the new ExoMol standards,[66] predissociation lifetimes of molecules are to be included into the ExoMol line lists by convolution with the radiative lifetimes τ_r as in Eq. (22).

The non-zero contribution of the continuum X $^2\Pi$ state levels to the line broadening of the A $^2\Sigma^+$ state levels has been reported and shows that a predissociation into the continuum associated with the ground electronic state is of a small but non-zero probability. In this case, this contribution is negligibly small; however, this may not be the case in all systems and warrants consideration in other predissociation studies. OH exhibits strong and complex predissociation dynamics through the interaction of three repulsive electronic states. It is, however, a streamlined example of this effect as the energetic limits of the repulsive states are the same as that of the ground state. This means that if one ignores asymptotic fine structure effects, the dissociation products are independent of the dissociation channel. As this method is generally applicable, molecules with more varied predissociation channels may be of interest for future branching ratio and lifetime studies.

SUPPLEMENTARY MATERIAL

The calculated predissociation lifetimes, a comparison with literature data, and the DUO input file are provided in the supplementary material.

ACKNOWLEDGMENTS

This work was supported by the European Research Council (ERC) under the European Union's Horizon 2020 research and innovation program through Advance Grant No. 883830 and the UK STFC under Grant No. ST/R000476/1. The authors acknowledge the use of the UCL Myriad High Performance Computing Facility (Myriad UCL) and associated support services, in the completion of this work.

AUTHOR DECLARATIONS

Conflict of Interest

The authors have no conflicts to disclose.

Author Contributions

G. B. Mitev: Conceptualization (equal); Data curation (equal); Formal analysis (equal); Investigation (equal); Methodology (equal); Software (equal); Visualization (equal); Writing – original draft (equal). **Jonathan Tennyson**: Conceptualization (equal); Funding acquisition (equal); Methodology (equal); Project administration (equal); Supervision (equal); Writing – review & editing (equal). **Sergei N. Yurchenko**: Conceptualization (equal); Methodology (equal); Software (equal); Writing – review & editing (equal).

DATA AVAILABILITY

The data that support the findings of this study are available within the article and its supplementary material. The full lifetime calculation code, BINSLT, is freely available at ExoMol GitHub.

REFERENCES

[1] G. Sun, X.-F. Zheng, Y. Qin, Y. Song, J. Zhang, J. M. Amero, and G. J. Vázquez, Chin. J. Chem. Phys. **33**, 129 (2020).
[2] W. Zhou, Y. Yuan, and J. Zhang, J. Chem. Phys. **119**, 9989 (2003).
[3] D. C. Radenović, A. J. van Roij, S.-M. Wu, J. Ter Meulen, D. H. Parker, M. P. van der Loo, L. M. Janssen, and G. C. Groenenboom, Mol. Phys. **106**, 557 (2008).
[4] J. B. Nee and L. C. Lee, J. Chem. Phys. **81**, 31 (1984).
[5] J. A. Joens, J. Phys. Chem. A **105**, 11041 (2001).
[6] R. G. Prinn, R. F. Weiss, B. R. Miller, J. Huang, F. N. Alyea, D. M. Cunnold, P. J. Fraser, D. E. Hartley, and P. G. Simmonds, Science **269**, 187 (1995).
[7] J. S. A. Brooke, P. F. Bernath, C. M. Western, C. Sneden, M. Afsar, G. Li, and I. E. Gordon, J. Quant. Spectrosc. Radiat. Transfer **168**, 142 (2016).
[8] R. Landman, A. Sanchez-Lopez, P. Molliere, A. Y. Kesseli, A. J. Louca, and I. A. G. Snellen, Astron. Astrophys. **656**, A119 (2021).
[9] S. O. M. Wright, S. K. Nugroho, M. Brogi, N. P. Gibson, E. J. W. de Mooij, I. Waldmann, J. Tennyson, H. Kawahara, M. Kuzuhara, T. Hirano, T. Kotani, Y. Kawashima, K. Masuda, J. L. Birkby, C. A. Watson, M. Tamura, K. Zwintz, H. Harakawa, T. Kudo, K. Hodapp, S. Jacobson, M. Konishi, T. Kurokawa, J. Nishikawa, M. Omiya, T. Serizawa, A. Ueda, S. Vievard, and S. N. Yurchenko, Astron. J. **166**, 41 (2023).
[10] T. Furtenbacher, S. T. Hegedus, J. Tennyson, and A. G. Császár, Phys. Chem. Chem. Phys. **24**, 19287 (2022).
[11] E. F. van Dishoeck and A. Dalgarno, J. Chem. Phys. **79**, 873 (1983).
[12] S. R. Langhoff, E. F. van Dishoeck, R. Wetmore, and A. Dalgarno, J. Chem. Phys. **77**, 1379 (1982).
[13] E. F. van Dishoeck, S. R. Langhoff, and A. Dalgarno, J. Chem. Phys. **78**, 4552 (1983).
[14] E. F. Van Dishoeck and A. Dalgarno, Icarus **59**, 305 (1984).
[15] C. W. Bauschlicher, Jr. and S. R. Langhoff, J. Chem. Phys. **87**, 4665 (1987).
[16] D. R. Yarkony, J. Chem. Phys. **97**, 1838 (1992).
[17] S. Lee and K. F. Freed, J. Chem. Phys. **87**, 5772 (1987).
[18] C. Kalyanaraman and N. Sathyamurthy, Chem. Phys. **187**, 219 (1994).
[19] S. Lee, Chem. Phys. Lett. **240**, 595 (1995).
[20] S. Lee, J. Chem. Phys. **103**, 3501 (1995).
[21] S. Lee, Chem. Phys. Lett. **243**, 250 (1995).
[22] S. Lee, J. Phys. Chem. **99**, 13380 (1995).
[23] S. Lee, J. Chem. Phys. **104**, 1912 (1996).
[24] E. F. van Dishoeck, M. C. van Hemert, A. C. Allison, and A. Dalgarno, J. Chem. Phys. **81**, 5709 (1984).
[25] M. P. J. van der Loo and G. C. Groenenboom, J. Chem. Phys. **123**, 074310 (2005).
[26] S. Srivastava and N. Sathyamurthy, J. Phys. Chem. A **118**, 6343 (2014).
[27] X. Qin, S. D. Zhang, and J. Korean, J. Korean Phys. Soc. **65**, 2017 (2014).
[28] G. Parlant and D. R. Yarkony, J. Chem. Phys. **110**, 363 (1999).
[29] J. Tennyson, L. Lodi, L. K. McKemmish, and S. N. Yurchenko, J. Phys. B: At., Mol. Opt. Phys. **49**, 102001 (2016).
[30] P. L. Raston, T. Liang, and G. E. Douberly, J. Phys. Chem. A **117**, 8103 (2013).
[31] E. L. Derro, I. B. Pollack, L. P. Dempsey, M. E. Greenslade, Y. Lei, D. Č. Radenović, and M. I. Lester, J. Chem. Phys. **122**, 244313 (2005).
[32] J. Brzozowski, P. Erman, and M. Lyyra, Phys. Scr. **17**, 507 (1978).
[33] J. A. Gray and R. L. Farrow, J. Chem. Phys. **95**, 7054 (1991).
[34] D. E. Heard, D. R. Crosley, J. B. Jeffries, G. P. Smith, and A. Hirano, J. Chem. Phys. **96**, 4366 (1992).
[35] J. J. L. Spaanjaars, J. J. ter Meulen, and G. Meijer, J. Chem. Phys. **107**, 2242 (1997).
[36] G. Sun, W. Zhou, X. Zheng, Y. Qin, Y. Song, Y. Yuan, and J. Zhang, Mol. Phys. **119**, e1837974 (2021).
[37] Y. Li and P.-Y. Zhang, J. Theor. Comput. Chem. **10**, 747 (2011).
[38] M. L. Sink, A. D. Bandrauk, and R. Lefebvre, J. Chem. Phys. **73**, 4451 (1980).
[39] J. Tennyson and S. N. Yurchenko, J. Quantum Chem. **117**, 92 (2017).
[40] G. B. Mitev, R. P. Brady, O. Smola, J. Tennyson, and S. N. Yurchenko, "Calculation of spin-orbit induced predissociation lifetimes in rovibronic states of diatomic molecules," Phys. Chem. Chem. Phys. (unpublished) (2024).
[41] H. J. Werner, P. J. Knowles, R. Lindh, F. R. Manby, and M. Schütz, MOLPRO, *a package of ab initio programs*, 2010, see http://www.molpro.net/.
[42] H.-J. Werner, P. J. Knowles, G. Knizia, F. R. Manby, and M. Schütz, Wiley Interdiscip. Rev.: Comput. Mol. Sci. **2**, 242 (2012).
[43] H.-J. Werner, P. J. Knowles, F. R. Manby, J. A. Black, K. Doll, A. Heßelmann, D. Kats, A. Köhn, T. Korona, D. A. Kreplin, Q. Ma, T. F. Miller, A. Mitrushchenkov, K. A. Peterson, I. Polyak, G. Rauhut, and M. Sibaev, J. Chem. Phys. **152**, 144107 (2020).
[44] H.-J. Werner and P. J. Knowles, J. Chem. Phys. **82**, 5053 (1985).
[45] S. R. Langhoff and E. R. Davidson, Int. J. Quantum Chem. **8**, 61 (1974).
[46] A. T. Patrascu, C. Hill, J. Tennyson, and S. N. Yurchenko, J. Chem. Phys. **141**, 144312 (2014).
[47] S. N. Yurchenko, L. Lodi, J. Tennyson, and A. V. Stolyarov, Comput. Phys. Commun. **202**, 262 (2016).
[48] R. J. Le Roy, J. Quant. Spectrosc. Radiat. Transfer **186**, 179 (2017).
[49] A. A. Šurkus, R. J. Rakauskas, and A. B. Bolotin, Chem. Phys. Lett. **105**, 291 (1984).
[50] G. B. Mitev, S. Taylor, J. Tennyson, S. N. Yurchenko, A. A. Buchachenko, and A. V. Stolyarov, Mon. Not. R. Astron. Soc. **511**, 2349 (2022).
[51] M. Meuwly and J. M. Hutson, J. Chem. Phys. **110**, 8338 (1999).
[52] S. Skokov, K. A. Peterson, and J. M. Bowman, Chem. Phys. Lett. **312**, 494 (1999).
[53] A. Kramida, Y. Ralchenko, J. Reader, and NIST ASD Team, NIST atomic spectra database (ver. 5.9), National Institute of Standards and Technology, Gaithersburg, MD, 2021, available at: http://physics.nist.gov/asd.
[54] G. Herzberg, *Spectra of Diatomic Molecules* (Krieger Publishing, 1989), pp. 223–257.
[55] T. Rivlin, L. K. McKemmish, K. E. Spinlove, and J. Tennyson, Mol. Phys. **117**, 3158 (2019).
[56] M. Pezzella, S. N. Yurchenko, and J. Tennyson, Phys. Chem. Chem. Phys. **23**, 16390 (2021).
[57] A. U. Hazi and H. S. Taylor, Phys. Rev. A **1**, 1109 (1970).
[58] V. A. Mandelshtam, T. R. Ravuri, and H. S. Taylor, Phys. Rev. Lett. **70**, 1932 (1993).
[59] Z. Bacic and J. Simons, J. Phys. Chem. **86**, 1192 (1982).
[60] D. T. Colbert and W. H. Miller, J. Chem. Phys. **96**, 1982 (1992).
[61] J. Brown, A.-C. Cheung, and A. Merer, J. Mol. Spectrosc. **124**, 464 (1987).
[62] R. J. Le Roy and Y. Huang, J. Mol. Struct.: THEOCHEM **591**, 175 (2002).
[63] R. J. Le Roy, J. Quant. Spectrosc. Radiat. Transfer **186**, 167 (2017).
[64] Y. Pavlenko, J. Tennyson, S. N. Yurchenko, M. R. Schmidt, H. R. A. Jones, Y. Lyubchik, and A. Suárez Mascareño, Mon. Not. R. Astron. Soc. **516**, 5655 (2022).
[65] J. Zhang, J. Tennyson, and S. N. Yurchenko, "PyExoCross}: a Python program for generating spectra and cross sections from molecular line lists," RAS Tech. Instrum (to be published).
[66] J. Tennyson, M. Pezzella, J. Zhang, and S. N. Yurchenko, RAS Tech. Instrum. **2**, 231 (2023).